nanomaterials

MDPI

Article

Synthesis and Characterization of Tetracycline Loaded Methionine-Coated $NiFe_2O_4$ Nanoparticles for Anticancer and Antibacterial Applications

Faten Eshrati Yeganeh [1], Amir Eshrati Yeganeh [2], Bahareh Farasati Far [3], Afsoun Mansouri [4], Belay Zeleke Sibuh [5], Saravanan Krishnan [6], Soumya Pandit [7], Walaa F. Alsanie [8], Vijay Kumar Thakur [9,10,11,*] and Piyush Kumar Gupta [7,12,*]

1 Department of Chemistry, Science and Research Branch, Islamic Azad University, Tehran 1477893855, Iran; ffyeganeh@gmail.com
2 Department of Microbiology, Noor Dahesh Institute of Higher Education, Meymeh 45789427600, Iran; amireshratiyegane@gmail.com
3 Department of Chemistry, Iran University of Science and Technology, Tehran 1684613114, Iran; bahar.ferasati@gmail.com
4 School of Pharmacy and Pharmaceutical Sciences, Tehran Medical Sciences, Islamic Azad University, Tehran 1477893855, Iran; afsoonmansori@yahoo.com
5 Department of Biotechnology, School of Engineering and Technology, Sharda University, Plot No. 32–34, Knowledge Park III, Greater Noida 201310, Uttar Pradesh, India; belayzeleke63@yahoo.com
6 Creative Carbon Labs Pvt. Ltd., Chennai 600113, Tamil Nadu, India; sara.krish87@gmail.com
7 Department of Life Sciences, School of Basic Sciences and Research, Sharda University, Plot No. 32–34, Knowledge Park III, Greater Noida 201310, Uttar Pradesh, India; sounip@gmail.com
8 Department of Clinical Laboratories Sciences, The Faculty of Applied Medical Sciences, Taif University, Taif 21944, Saudi Arabia; w.alsanie@tu.edu.sa
9 Biorefining and Advanced Materials Research Centre, Scotland's Rural College (SRUC), Kings Buildings, Edinburgh EH9 3JG, UK
10 School of Engineering, University of Petroleum & Energy Studies (UPES), Dehradun 248007, Uttarakhand, India
11 Centre for Research & Developments, Chandigarh University, Mohali 140413, Punjab, India
12 Department of Biotechnology, Graphic Era Deemed to be University, Dehradun 248002, Uttarakhand, India
* Correspondence: vijay.thakur@sruc.ac.uk (V.K.T.); dr.piyushkgupta@gmail.com (P.K.G.)

check for updates

Citation: Yeganeh, F.E.; Yeganeh, A.E.; Far, B.F.; Mansouri, A.; Sibuh, B.Z.; Krishnan, S.; Pandit, S.; Alsanie, W.F.; Thakur, V.K.; Gupta, P.K. Synthesis and Characterization of Tetracycline Loaded Methionine-Coated $NiFe_2O_4$ Nanoparticles for Anticancer and Antibacterial Applications. *Nanomaterials* **2022**, *12*, 2286. https://doi.org/10.3390/nano12132286

Academic Editor: Jose L. Arias

Received: 19 May 2022
Accepted: 1 July 2022
Published: 3 July 2022

Publisher's Note: MDPI stays neutral with regard to jurisdictional claims in published maps and institutional affiliations.

Abstract: In the present study, nickel ferrite ($NiFe_2O_4$)-based smart magnetic nanoparticles were fabricated and coated with methionine. Physiochemical characterization of the obtained Met-$NiFe_2O_4$ nanoparticles revealed the presence of methionine coating over the nanoparticle surface. Drug release study indicated that Tet-Met-$NiFe_2O_4$ nanoparticles possess pH-responsive controlled drug release behavior for tetracycline (Tet). The drug loading content for Tet was found to be 0.27 mg/L of nanoparticles. In vitro cytotoxicity test showed that the Met-$NiFe_2O_4$ nanoparticles is biocompatible. Moreover, this magnetic nanostructured material shown strong anticancer property as these nanomaterials significantly reduced the viability of A375 cells when compared to free Tet solution. In addition, Tet-Met-$NiFe_2O_4$ nanoparticles also showed strong antibacterial activity against different bacterial pathogens.

Keywords: methionine-$NiFe_2O_4$ nanoparticles; drug release; antibacterial; anticancer; cytotoxicity

1. Introduction

In today's world, hospital-acquired infections caused by viral, bacterial, and fungal pathogens remain the primary concern and biggest challenge among the healthcare workers [1–5]. Antimicrobial molecules include antibiotics and biocides having a bactericidal/bacteriostatic effect on bacteria. Antibiotic is an active substance of synthetic or natural origin which is used to eradicate bacterial infections in humans or animals. While biocide is an active chemical molecule to control the growth of or kill bacteria. Hence, antimicrobial

activity exhibits an inhibitory or lethal effect of a biocidal product or an antibiotic [6–9]. Biocides and antibiotics may share some common behavior and properties in their respective activity and in the resistance mechanisms developed by bacteria. Today, it is important to weigh the risks of selecting antibiotic resistant bacteria by biocide use correctly and to have a clear view of the corresponding emerging health risk. Moreover, understanding the selection and dissemination of biocide resistant pathogens is very important for combating the dissemination of health care associated diseases and foodborne pathogens.

Antibiotics are broadly classified as antibacterial, antifungal, or antiviral drugs depending on their target group [6–8]. For many decades, antibiotics are widely utilized in medical procedures ranging from organ transplants to chemotherapy [10]. From this, the significance of antibiotics is understood as it protects the host cells from microbial or viral infections [11,12]. Towards this, an antibiotic, Tetracycline (Tet), has been extensively used to treat various bacterial infections [13,14]. In addition, Tet is a well-recognized antibiotic used in the treatment of skin cancer and shown to inhibit several other cancer types.

The functional role of antibiotics is mainly based on the drug delivery system and the mechanism of their controlled delivery to targeted affected cells [15–18]. Recently, several organic-inorganic hybrid nanoparticles have been extensively used in anticancer therapy. Indeed, methionine is one of the essential amino acids i.e., required for the human growth due to its antioxidant activity. The activated functional groups of methionine (-COOH and -NH_2) are used to conjugate the metal atoms, and further the loading and release behavior are investigated. The design and synthesis of organic–inorganic hybrid nanoparticles through combining the advantages of both organic and inorganic counterparts may improve the overall properties, such as particle size, surface charge, and many other physicochemical properties [19,20]. Roca et al. (2012) reported that modified magnetic NPs (MNPs) has shown increased efficacy under in vivo conditions [21].

Several recent findings have emphasized the therapeutic role of MNPs in treating the disease [22–24]. Nanoparticles whose particle size ranging between 10–100 nm have shown properties to improve drug bioavailability and facilitate the targeted accumulation of drugs inside the cell through enhanced permeability and retention (EPR) effect [25,26]. Magnetic spinel ferrite nanoparticles are widely used in biotechnology. The main advantage of magnetic nanoparticles is that can be readily isolated from the solution media using an external magnetic field. $NiFe_2O_4$ nanoparticles have gained worldwide acceptance due to their low coercivity, high saturation magnetization, excellent chemical stability, high Curie temperature, and electromagnetic performance [27]. However, to the authors' best knowledge, the utilization of $NiFe_2O_4$ magnetic nanoparticles in the field of biomedicine is available. Further, $NiFe_2O_4$ nanoparticles are widely used as an in vivo magnetic hyperthermia agent in biomedicine [28]. $NiFe_2O_4$ nanoparticles exhibited an inverse spinel structure with Ni^{+2} in octahedral sites (Ni(OH)) and Fe^{+3} equally distributed between tetrahedral (Fe (Td)) and octahedral sites (Fe(OH)) of the O^{2-} FCC (Face-Centered Cubic) cell [29]. The complete crystalline structure belongs to O_h^7 space group with oxygen atoms occupying the 32e positions, Fe (Td) atoms occupying the 8a ones and the Ni(OH) and Fe(OH) atoms are distributed on 16d positions [30]. Different methods, including solvothermal, sol-gel, co-precipitation, microemulsion, and thermal decomposition, have been utilized to fabricate magnetic nanostructures of varying morphologies and structural variants [31–34] which has immense scope and applications in biomedical science.

Various amino acids have been successfully applied in the preparation of magnetic nanoparticles. However, the use of methionine in the fabrication of nickel-ferrite based nanocomposite is not reported yet. Recently, Saykova et al. synthesized magnetic $NiFe_2O_4$@Au crystal nanoparticles using the amino acid methionine as a reducing and stabilizing agent [35]. The nanoparticles obtained in this study after three stages of gold deposition had an average particle size of about 120 nm, which is relatively large for cellular adsorption studies and for biomedical applications thereof. In this study, methionine-coated nickel ferrite nanoparticles with an average particle size of about 27 nm are synthesized

in a simple and cost-effective step by reflux method, which is the preferred magnetic nanomaterial for various biological applications.

Recently, non-coated nickel ferrite magnetic nanoparticles were synthesized by Majed et al. and tested in a rat model [36]. However, tetracycline loading on this nanostructure (Met-$NiFe_2O_4$), and its effect on normal and A-375 cancer cells has not been studied. In addition, the loading of tetracycline on Met-$NiFe_2O_4$ as a biocompatible and targeted nanocarrier and its effect on bacterial growth remain unexplored. Compared to previous literature, it can be concluded that we have prepared nickel ferrite nanoparticles coated with methionine in a facile synthetic route which is explored for anticancer and antibacterial applications.

In the present study, a simple and effective strategy is developed to synthesize Met-$NiFe_2O_4$ nanoparticles employing a one-step reflux procedure. Various characterization studies are performed to examine the shape, structure, and magnetic characteristics of Met-$NiFe_2O_4$ nanoparticles. Tet antibiotic is used to explore the drug loading and release profile of Met-$NiFe_2O_4$ nanoparticles, for the first time. Moreover, MTT tests are used to assess the in vitro cytotoxicity of Met-$NiFe_2O_4$ nanoparticles before and after Tet loading of varying doses and incubation periods. Furthermore, antibacterial activity of Met-$NiFe_2O_4$ nanoparticles against pathogenic bacteria is assessed. To date, the cytotoxicity and antibacterial properties of Met-$NiFe_2O_4$ nanoparticles have not been reported.

2. Materials and Methods

2.1. Materials

Ferric chloride hexahydrate ($FeCl_3 \cdot 6H_2O$), Nickel chloride hexahydrate ($NiCl_2 \cdot 6H_2O$), sodium hydroxide, methionine, and other chemicals were procured from Merck, Germany. A-375 and HFF cells were obtained from the Pasteur cell bank. *Staphylococcus aureus* (ATCC 23235), *Escherichia coli* (ATCC 25922), *Pseudomonas aeruginosa* (ATCC 15442), and *Enterococcus faecalis* (ATCC 29212) strains were collected from The Pasteur Institute of Iran.

2.2. Fabrication of Met-$NiFe_2O_4$ Nanoparticles

Met-$NiFe_2O_4$ nanoparticles were synthesized by reflux method (as shown in Figure 1). In brief, 2.431 g of $FeCl_3 \cdot 6H_2O$ and 1.069 g of $NiCl_2 \cdot 6H_2O$ were dissolved in 120 mL of distilled water (d.H_2O), followed by the addition of 1.5 M NaOH solution to adjust the pH to 12. Then, a brown colored solution appeared, and was filtered and washed several times with d.H_2O until the pH of the filtrate becomes neutral (7). Next, 1.5 g of methionine was added. The resulting mixture was heated to 70–80 °C and refluxed for 3 h. The final product was collected by strong magnetic separation and rinsed three times with absolute ethanol and d.H_2O. In a similar way, $NiFe_2O_4$ nanoparticles were synthesized, but without methionine.

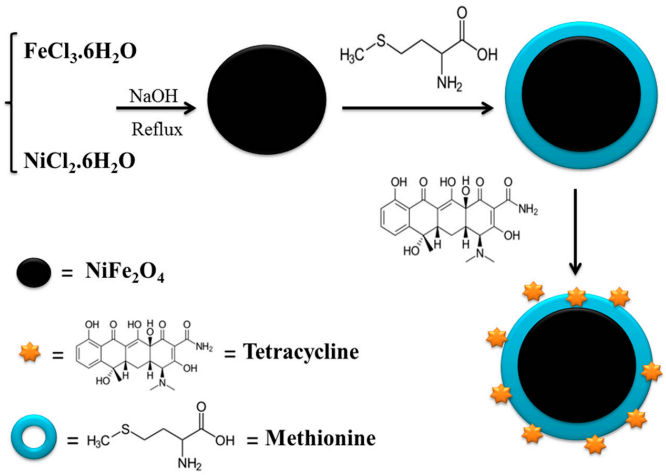

Figure 1. Synthesis and Tet loading on Methionine-coated nickel ferrite nanoparticles (Met-$NiFe_2O_4$ nanoparticles).

2.3. Physicochemical Characterization Studies

X-ray diffraction (XRD) analysis $NiFe_2O_4$ and Met-$NiFe_2O_4$ nanoparticles was carried out using the STOE STADI-P instrument (STOE, & Cie GmbH, Darmstadt, Germany). Field Emission-Scanning Electron Microscopy (FESEM) (Zeiss-EHT-10.00 kV, Carl Zeiss SMT AG Company, Oberkochen, Germany) and High Resolution-Transmission Electron Microscopy (HR-TEM) (Zeiss-EM10C-100 kV, Carl Zeiss SMT AG Company, Oberkochen, Germany) instruments were used to determine morphology and particle size of nanoparticles respectively. The particle size was measured in a dry state through the particle size distribution curve. Next, Fourier Transform Infrared Spectroscopy (FTIR) (Nexus 870, Nicolet, Madison, WI, USA) was also performed. Absorbance measurements at 275 nm through means of UV/visible spectroscopy (Shimadzu UVS-1700, Shimadzu Corporation, Kyoto, Japan) was employed to study the amount of drug adsorbed on nanoparticle surface and the controlled drug release behavior. Thermal properties were analyzed by Thermogravimetric Analyzer (TGA) (Shimadzu TA Q600, Shimadzu TA Instrument SDT Q600, New Castle, DE, USA) in a temperature range of 25 to 800 °C under Nitrogen atmosphere at a constant heating rate. Finally, the magnetic properties were studied by Quantum Design MPMS-XL-7 instrument (MPMS-XL-7), San Diego, CA, USA.

2.4. Average Hydrodynamic Size and Zeta Potential Measurement

The average hydrodynamic size (Z-average) (based on light diffraction), particle size distribution (PDI), and average zeta potential (based on electrophoretic movement of particles) of $NiFe_2O_4$, Met-$NiFe_2O_4$ and Tet-Met-$NiFe_2O_4$ nanoparticles were determined by Malvern Zetasizer 2000 HS instrument (Malvern, UK) where nanoparticles were diluted 100 times in distilled water at 25 ± 0.1 °C prior to experiment.

2.5. Tetracycline Loading and Release Behavior

Various concentrations of Tet were added to 0.2 mg of Met-$NiFe_2O_4$ nanoparticles and incubated in the dark conditions for 24 h at room temperature. The resulting Tet-Met-$NiFe_2O_4$ nanoparticles were pelleted using centrifuge, and the collected supernatant was subjected to absorbance measurements at 275 nm using UV/Visible spectroscopy to determine the drug loading efficiency of Tet (Figure 1).

Next, 10 mg of Tet-Met-$NiFe_2O_4$ nanoparticles was suspended into 10 mL of PBS buffer of pH 5 and 7.4 at 37 °C under dark conditions. Then, 1 mL supernatant was collected at different time intervals and replaced with fresh PBS. Finally, the concentration of released Tet was calculated using UV/Visible spectroscopy (Shimadzu UVS-1700, Shimadzu Corporation, Kyoto, Japan). The drug release data were fitted with different kinetic models' equations for determining the mechanism of drug release from Tet-Met-$NiFe_2O_4$ nanoformulations. The most appropriate drug release kinetic model was determined by analyzing the regression coefficients of graphs. According to this, the drug release mechanism was determined from the drug delivery system.

2.6. In Vitro Cytotoxicity

A standard MTT test was performed to analyze the in vitro cytotoxicity of Tet-Met-$NiFe_2O_4$ nanoparticles on A375 and HFF cell lines. These cell lines were cultured using RPMI-1640 fresh medium supplemented with 10% FBS and 1% penicillin/streptomycin in a humid CO_2 incubator with 5% carbon dioxide at 37 °C. Once the cells had achieved 85–95% confluence, the media was aspirated. Detachment of the cell monolayer was performed using trypsin-EDTA (0.25% (*w*/*v*)). Then, the detached cells were resuspended in a complete growth medium, labeled with trypan blue, and counted using hemocytometer. Different concentrations of Tet-Met-$NiFe_2O_4$ (0–70 μg/mL) were added to the cultured A375 and HFF cells and incubated for 72 h. For cell proliferation studies, the cells were incubated with 0.5 mg/mL of MTT reagent for 4 h. Then, the purple crystal formazan formed was dissolved in 100 μL of DMSO for the colorimetric determination of the cells' oxidoreductase enzymatic activity. The absorbance values of both control and test concentrations were

measured at 570 nm while reference blank measurements taken at 630 nm, and then the cell viability and IC_{50} values were calculated [7,15,37]. The percentage of cell viability was calculated using Equation (1).

$$Cell\ Viability\ (\%) = \frac{absorbance\ of\ treated\ cells}{absorbance\ of\ control\ cells} \times 100 \quad (1)$$

2.7. Antibacterial Activity

The antibacterial activities of free Tetracycline and Tet-Met-$NiFe_2O_4$ nanoparticles were evaluated against both Gram-positive and Gram-negative bacteria, such as *E. coli*, *P. aeruginosa*, *S. aureus*, and *E. faecalis*, using microdilution method. Next, the obtained data was used to calculate the minimum bactericidal concentrations (MBC) and minimum inhibitory concentrations (MIC). Different samples were initially made using Mueller–Hinton Broth (MHB), then 100 µL of each sample was added into 96-well microplates. Approximately 0.5 McFarland standard bacterial suspension was prepared and diluted in Mueller–Hinton Broth to achieve a final concentration of 1×10^6 colony forming units (CFU)/mL. Then, 100 µL of diluted bacterial suspension was mixed with 100 µL of samples (with different concentrations as mentioned above) in 96-well microplates and incubated at 37 °C for 18 h. Bacterial suspension without the drug acts as positive control, while the negative control was the highest drug concentration without bacteria. MBC test was performed to confirm the results of MIC test. Consequently, 100 µL of clear wells with no visible bacterial growth was transferred to petri plates containing MHA (Mueller–Hinton Agar) medium and incubated for overnight at 37 °C [7,8].

2.8. Statistical Analysis

All tests were performed in triplicates (n = 3) and each test repeated at least three independent times. The equality of variance and normality were checked by Brown–Forsythe and Shapiro–Wilk tests, respectively. Then, the data was compared using one way or two-way analysis of variance (ANOVA) with repeated measures, followed by Tukey's or Sidak's post hoc comparison test. The results were given as mean ± SD. The differences were considered significant when a p-value of less than 0.05 is considered statistically significant. * $p < 0.05$, ** $p < 0.01$, *** $p < 0.001$.

3. Results and Discussion

3.1. Synthesis and Physicochemical Characterizations of Tet-Met-$NiFe_2O_4$ Nanoparticles

3.1.1. XRD Analysis

The method of fabrication of Met-$NiFe_2O_4$ nanoparticles is outlined in Figure 1. XRD analysis showed the diffraction peaks of crystal spinel $NiFe_2O_4$ nanoparticles at 18.60°, 30.49°, 35.88°, 37.45°, 43.60°, 53.98°, 57.54°, and 63.12° 2θ values (JCPDS No. 98-006-0930) while in the case of Met-$NiFe_2O_4$ nanoparticles, the diffraction peaks were observed at 18.57°, 30.24°, 35.73°, 37.44°, 43.32°, 53.69°, 57.28°, and 62.77° 2θ values (JCPDS No. 98-006-0930) (Figure 2A). The entry of methionine into the network cavity and an increase in network space is reflected through a drip in 2θ value corresponding to crystal spinel $NiFe_2O_4$ nanoparticles. The characteristic diffraction peaks for two samples are indexed to the crystal planes of (111), (220), (311), (222), (400), (422), (511), and (440). Met-$NiFe_2O_4$ nanoparticles with average size of 27 nm as calculated from the full-width value at half maximum (FWHM) of broadened characteristic peaks using Debye–Scherrer's Equation (2).

$$D = \frac{0.9\lambda}{FWHM\ \cos\theta} \quad (2)$$

where D denotes the crystalline size, β is the full width at half maximum (FWHM), θ represents the Bragg angle corresponding to the peak, and λ is the wavelength of the X-rays.

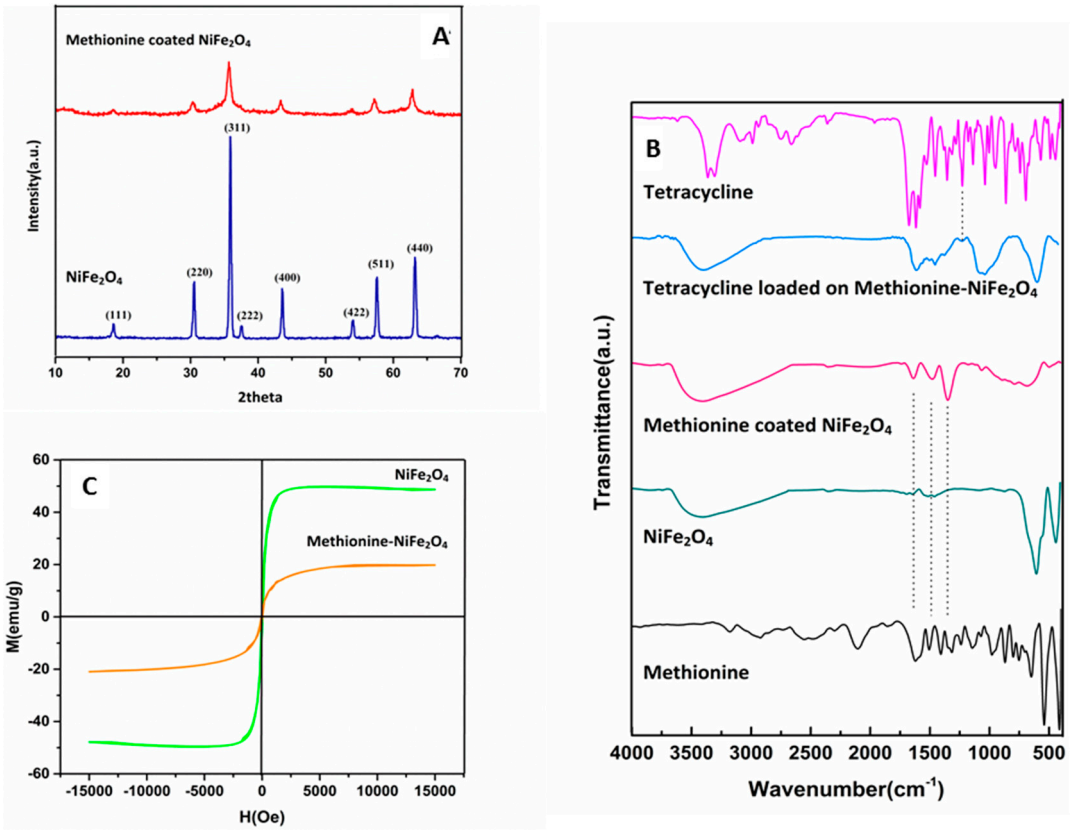

Figure 2. X-ray diffraction patterns of $NiFe_2O_4$ nanoparticles with and without methionine coating (**A**), FTIR spectrum of methionine, Tet, $NiFe_2O_4$ nanoparticles, Met-$NiFe_2O_4$ nanoparticles, Tet-Met-$NiFe_2O_4$ nanoparticles, (**B**) and Magnetization curves of $NiFe_2O_4$ and Met-$NiFe_2O_4$ nanoparticles (**C**).

3.1.2. FT-IR Spectral Analysis

FTIR analysis was used to study the nature of functional groups present on the surface of MNPs. The FTIR spectra of methionine, free Tet, bare $NiFe_2O_4$, Met-$NiFe_2O_4$ nanoparticles, and Tet-Met-$NiFe_2O_4$ nanoparticles are shown in Figure 2B. The Methionine amino acid spectrum is a combination of carboxylate salts and the first type amine. The symmetric and asymmetric N-H bending assigned in the region at 1517 cm^{-1} and 1630 cm^{-1} respectively. Furthermore, the symmetric and asymmetrical stretching of the COO^- bond was exhibited at 1419 cm^{-1} and 1600 cm^{-1}, respectively [38]. C–O bond represented at 1232–1330 cm^{-1}. The inherent vibration of tetrahedral and octahedral metal-oxygen complexes of $NiFe_2O_4$ is ascribed to regions observed at 400 and 600 cm^{-1}, respectively, which are mostly dependent on Fe–O distance [38].

FTIR spectrum of Met-$NiFe_2O_4$ nanoparticles revealed that methionine was present on the surface of $NiFe_2O_4$ nanoparticles. Tet features two small vibration at 500–569 cm^{-1} in its FT-IR spectra, which is linked to out-of-plane ring deformation. The regions at 1000–1257 cm^{-1} are associated with C–H in-plane deformation vibrations, while those at 998 cm^{-1} are associated with C–N stretching. Two bands appeared at 1462 and 1366 cm^{-1} displaying the bending vibrations of C–H and CH_3 groups, respectively. Band of C=C stretching is observed at 1571–1632 cm^{-1}. C–H and CH_3 stretching are attributed to the vibrational at 3013–3078 cm^{-1} and 2819–2949 cm^{-1}. Bands of N-H and O-H stretching is ascribed to the regions which seen at 3319–3340 cm^{-1} [39]. After Tet loading, the regions at 998–1257 cm^{-1} were originated in the FTIR spectrum, which is most likely due to C–N stretching and C–H vibration bands in-plane deformation of Tet. These findings supported that methionine's gets effectively coated onto MNPs, and, thus, possess good potential for drug loading and acts as smart nanocarrier for drug delivery.

3.1.3. Magnetic Property Analysis

Figure 2C displayed the magnetic properties of bare $NiFe_2O_4$ and Met-$NiFe_2O_4$ nanoparticles at room temperature in a magnetic field ranging from −15 kOe to 15 kOe. These MNPs exhibited the superparamagnetic behavior. The saturation magnetization (Ms) of bare $NiFe_2O_4$ and Met-$NiFe_2O_4$ nanoparticles were calculated to be 47.56 and 19.80 emu/g, respectively. Further, the saturation magnetization (Ms) of Met-$NiFe_2O_4$ nanoparticles was also reduced at room temperature. Superparamagnetic behavior is an important feature for biomaterials, which facilitate their tracking in the magnetic field while keeping the advantage of a stable and homogeneous suspension during drug delivery.

3.1.4. Size and Morphology Analysis

FE-SEM (Figure 3A) and HR-TEM (Figure 3B,C) images indicated that $NiFe_2O_4$ nanoparticles, Met-$NiFe_2O_4$ nanoparticles, and Tet-Met-$NiFe_2O_4$ nanoparticles, were found to be spherical in shape and possess nearly uniform sizes. Besides this, the TEM images of Met-$NiFe_2O_4$ and Tet-Met-$NiFe_2O_4$ nanoparticles showed a mild aggregation, probably due to the strong magnetic interactions between the $NiFe_2O_4$ nanoparticles. Methionine was successfully coated onto the surface of $NiFe_2O_4$ nanoparticles, and the particle size was calculated to be 28–29 nm.

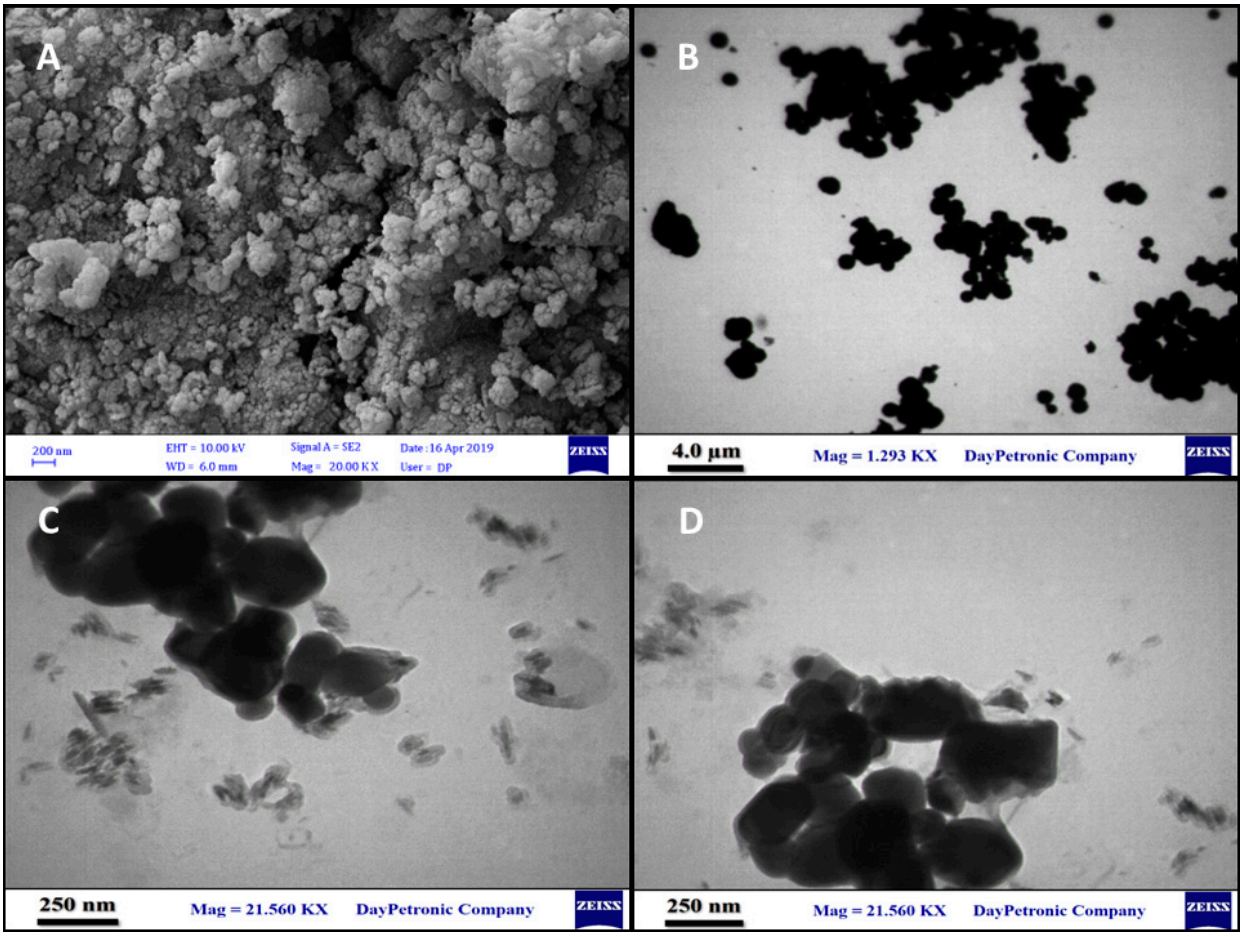

Figure 3. FE-SEM of Met-$NiFe_2O_4$ nanoparticles (**A**), TEM images of $NiFe_2O_4$ nanoparticles (**B**), Met-$NiFe_2O_4$ nanoparticles (**C**), and Tet-Met-$NiFe_2O_4$ nanoparticles (**D**).

3.1.5. Thermogravimetric Analysis

Thermogravimetric analysis (TGA) of methionine, $NiFe_2O_4$ nanoparticles, and Met-$NiFe_2O_4$ nanoparticles (Figure 4) were recorded. TGA profile showed that the initial weight loss observed at 150 to 260 °C could be due to thermal decomposition of carbon

dioxide, water and fine molecules trapped between the layers. On the other hand, heat-induced thermal degradation of methionine could be noticed at 260–300 °C, which is also consistent with TGA profile of amino acid, methionine. Further increase in temperature above 350 °C showed no change in weight which could be due to the high stability of the nanostructure [33,40]. The weight loss observed near 300 °C for $NiFe_2O_4$ nanoparticles and Met-$NiFe_2O_4$ nanoparticles were found to be 8.3% and 13.8%, respectively. Difference in the weight loss between $NiFe_2O_4$ nanoparticles and Met-$NiFe_2O_4$ nanoparticles near 300 °C indicated that methionine was successfully coated onto the surface of the $NiFe_2O_4$ nanoparticles.

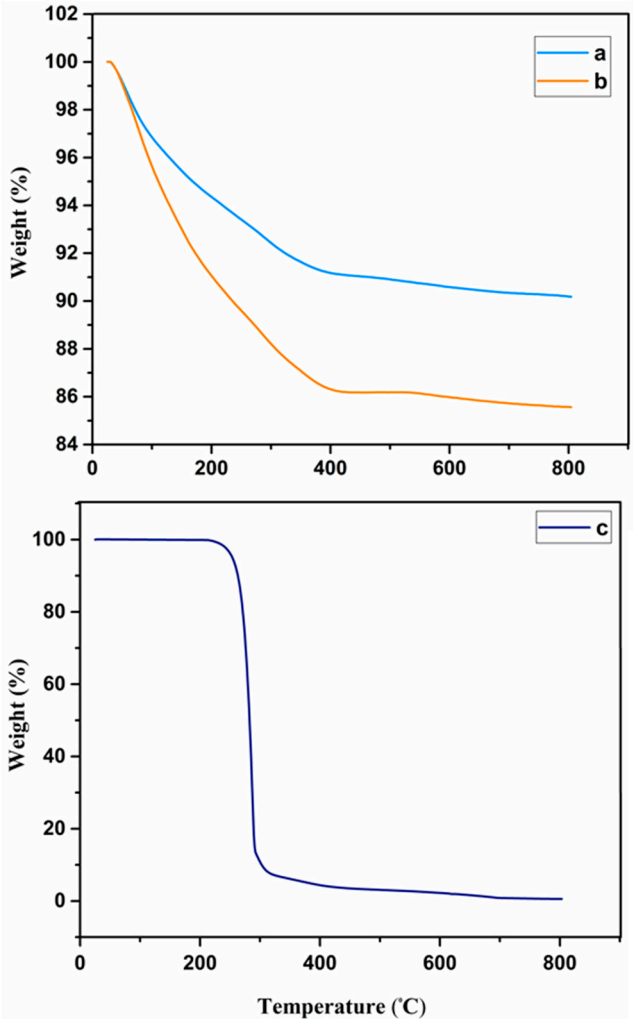

Figure 4. Thermogravimetric curves of $NiFe_2O_4$ nanoparticles (**a**), Met-$NiFe_2O_4$ nanoparticles (**b**), and methionine (**c**).

3.2. Size Distribution and Zeta Potential Measurement

The average hydrodynamic size, particle size distribution, and average zeta potential of all nanoparticles were measured at the same concentration and pH values. The particle hydrodynamic size distribution graph was plotted using Gaussian theorem for $NiFe_2O_4$, Met-$NiFe_2O_4$, and Tet-Met-$NiFe_2O_4$ nanoparticles (Figure 5). All the calculated values are given in a tabulated form (Table 1).

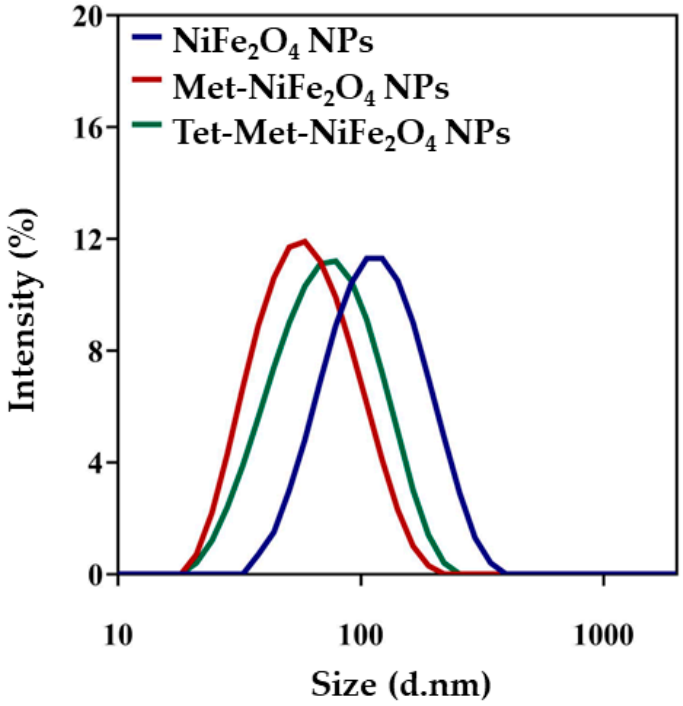

Figure 5. The particle hydrodynamic size distribution curves of $NiFe_2O_4$, Met- $NiFe_2O_4$, and Tet-Met-$NiFe_2O_4$ nanoparticles.

Table 1. Average hydrodynamic Size, PDI, and average zeta potential values of the fabricated formulations.

Formulation	Size (d.nm)	PDI	Zeta Potential (mV)
$NiFe_2O_4$	168.5 ± 11.8	0.346 ± 0.02	−32.4 + 2.4
Met-$NiFe_2O_4$	72.4 ± 8.8	0.247 ± 0.06	−27.7 ± 4.3
Tet-Met-$NiFe_2O_4$	90.9 ± 10.6	0.323 + 0.02	−31.6 ± 1.2

3.3. Drug Loading and Release Study

Tet was further loaded onto Met-$NiFe_2O_4$ nanoparticles, and the drug loading and release profile was assessed. As shown in Figure 6A, the maximum loading capacity of Met-$NiFe_2O_4$ nanoparticles reached 0.055 mg/mg, when the initial Tet concentration was 0.09 mg/mL. In other words, 0.27 mg of Tet was loaded onto 1 mg of nanocarrier. The amount of drug loading is enhanced through increasing the initial drug concentration taken for the study. This is possible due to the larger surface area and hydrogen bonding between Tet and Met-$NiFe_2O_4$ nanoparticles. To evaluate the drug release profile, the Tet-Met-$NiFe_2O_4$ nanoparticles were suspended in the buffer media of pH 5 and 7.4. Figure 6B shows the pH-dependent release of Tet from Met-$NiFe_2O_4$ nanoparticles. Drug release was observed at pH values near the tumor's environment (pH 5), while the lower drug release was detected at pH 7.4. The pH-sensitive drug release of the nanocarrier under neutral conditions (pH 7.4) could reduce the drug loss during blood transportation and lessen the side effects of anti-cancer drugs observed in normal cells. In the simulated environment of tumors (pH 5), this above-mentioned property of nanomaterial facilitates efficient anti-cancer drug release [41]. The pH-responsive nano-based delivery tools could lead to site-specific release of therapeutic cargos through cleaving pH-sensitive bonds across the pH gradient and augment an increase in toxicity under acidic conditions prevalent in the tumor regions [42,43].

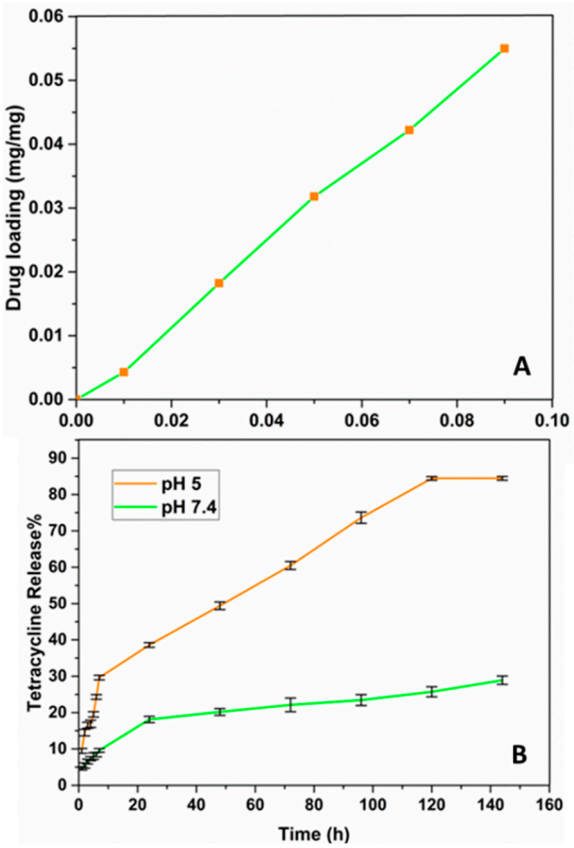

Figure 6. Tet loading on Met-$NiFe_2O_4$ nanoparticles (**A**) and Tet release from Met-$NiFe_2O_4$ nanoparticles at different pH values (**B**).

At neutral and acidic pH, the release kinetics of drug-loaded Met-$NiFe_2O_4$ nanoparticles were assessed using zero-order, first-order, Higuchi, and Korsmeyer–Peppas models, as shown in Table 2. An ideal kinetic model with a higher linear regression coefficient (close to 1) and determination (R^2) describe the drug release mechanism in the best way. The Higuchi model and Korsmeyer–Peppas model described the release kinetics at pH 5 and pH 7.4 ($n < 0.45$), whereas the Korsmeyer–Peppas model indicated the Fickian diffusion mechanism. It is worth mentioning that the drug gets distributed through diffusion in these cases (Higuchi model and Fickian diffusion mechanism). The pH-dependent drug release is well suited for cancer therapy, where the cancerous cells have an acidic intercellular environment while the healthy cells do not. The mathematical analysis is illustrated at pH 7.4 and pH 5 in Figures 7 and 8.

Table 2. The drug release kinetic models and the parameters obtained for optimum nanoformulation.

Kinetic Models	Equation	R^2	
		Met-$NiFe_2O_4$ Nanoparticles (pH—7.4)	**Met-$NiFe_2O_4$ Nanoparticles (pH—5)**
Zero-Order	$C_t = C_0 + K_0t$	0.8906	0.9516
First-Order	$LogC = LogC_0 + K_t/2.303$	0.9080	0.9809
Higuchi	$Q = K_h\sqrt{t}$	0.9712	0.9885
Korsmeyer-Peppas	$M_t/M_\infty = Kt^n$	0.9879 (*n = 0.3775)	0.9852 (*n = 0.4261)

* Diffusion or release exponent.

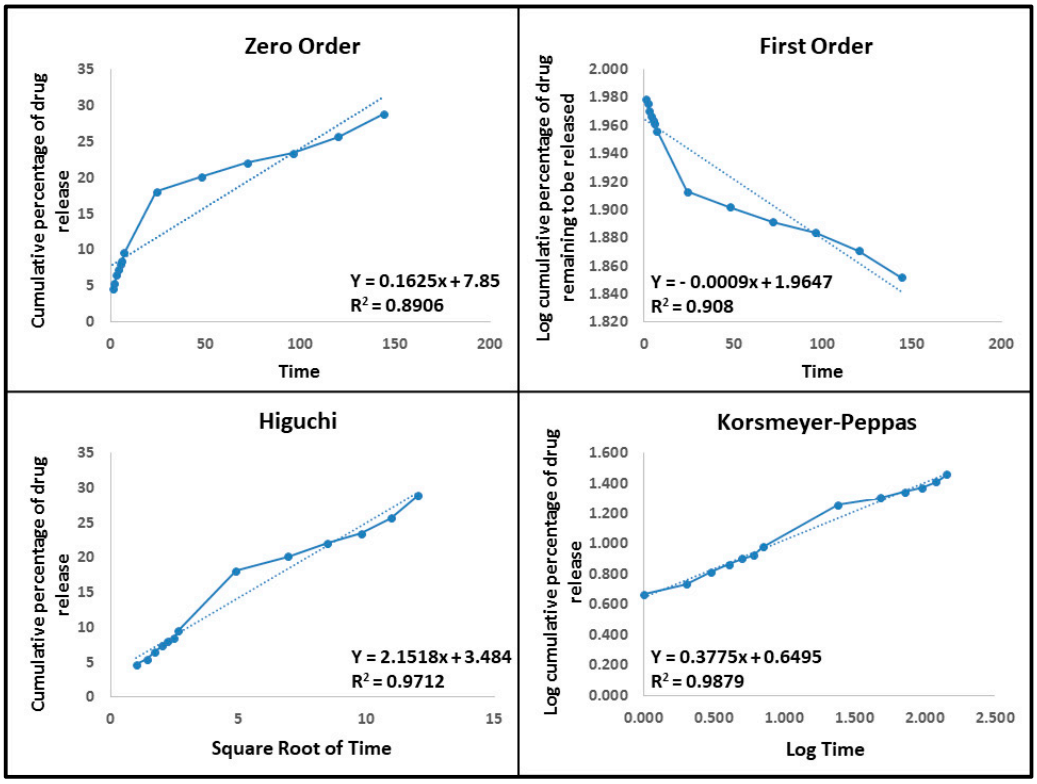

Figure 7. Drug release kinetic models like zero-order, first-order, Higuchi, and Korsmeyer–Peppas models used to study the tetracycline release from Tet-Met-$NiFe_2O_4$ nanoparticles at pH 7.4.

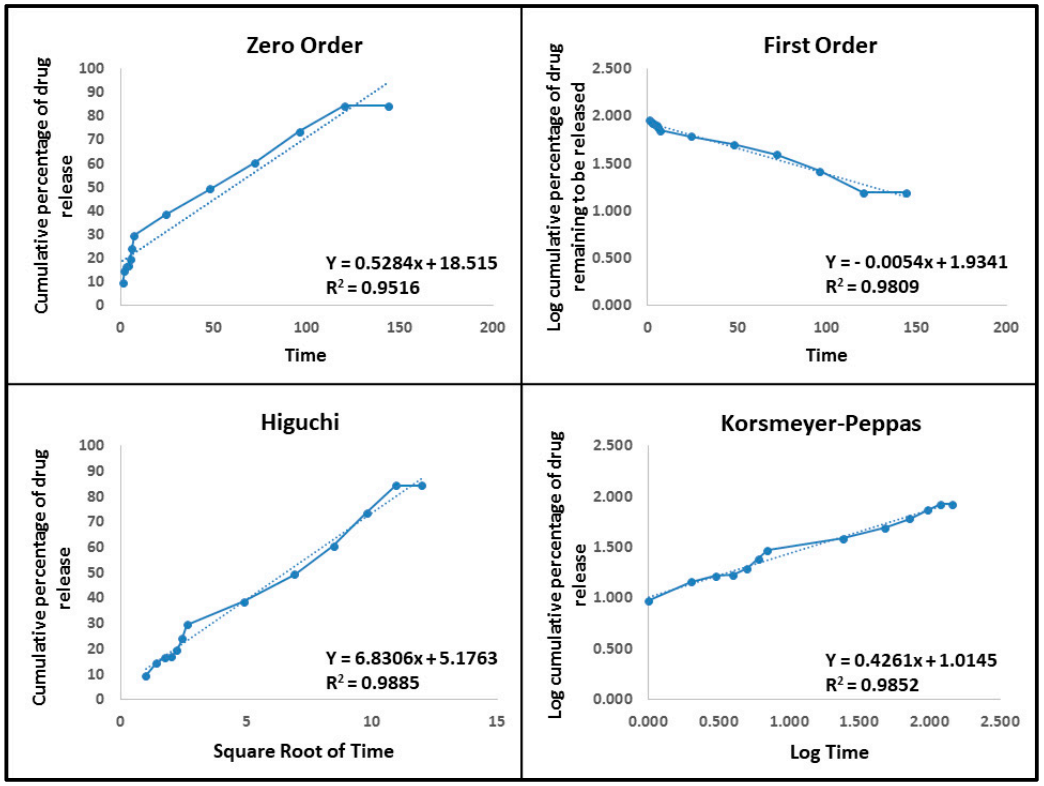

Figure 8. Drug release kinetic models like zero-order, first-order, Higuchi, and Korsmeyer–Peppas models used to study the tetracycline release from Tet-Met-$NiFe_2O_4$ nanoparticles at pH—5.

3.4. Cytotoxicity Studies

The cytotoxicity of Tet-Met-$NiFe_2O_4$ nanoparticles and free Tet were investigated using MTT test thrice for the concentration range of 0–70 µg/mL. Melanoma (A375 cells) and Human Foreskin Fibroblasts (HFF cells) were selected for the MTT assay. Results indicated that both free Tet and Tet-Met-$NiFe_2O_4$ nanoparticles showed cytotoxicity on cancer cells while toxicity was not observed with normal cells. As shown in Figure 9B, the cytotoxicity of Tet-Met-$NiFe_2O_4$ nanoparticles (IC_{50} = 32.55 ± 7.31 µg/mL) was higher than free Tet (IC_{50} = 76.58 ± 5.78 µg/mL) at 72 h. One possible reason for the differences in toxicity is due to difference in intracellular uptake of drug between the free drug and drug-loaded nanoparticles. More importantly, when the free drug is taken by cells, its release is faster, which means it is available to cell in less time owing to cross-sectional effect. When the drug is loaded onto nanoparticles, it exhibits controlled release, sustained effect, and as a result, the overall therapeutic efficacy is significantly improved [22,44]. Furthermore, Tet-Met-$NiFe_2O_4$ nanoparticles displayed no cytotoxicity on HFF cells (Figure 9A) due to excellent biocompatibility observed through coating the MNPs with amino acid methionine. These results finally showed that the biocompatible Tet-Met-$NiFe_2O_4$ nanoparticles synergistically improved the growth inhibitory effect on cancer cells.

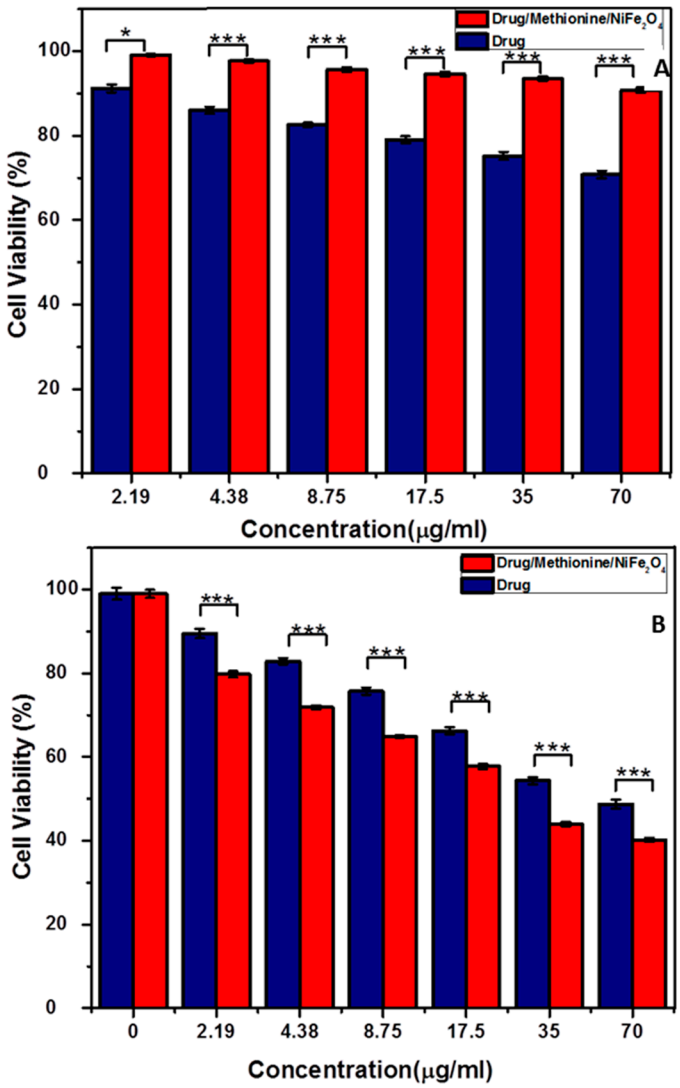

Figure 9. Cell viability of Tet-Met-$NiFe_2O_4$ nanoparticles and free Tet solution after 72 h incubation with (**A**) HFF cells and (**B**) A375 cells. The data is expressed as mean ± SD (n = 5). * $p < 0.05$, *** $p < 0.001$.

3.5. Antibacterial Activity

Microdilution method was used to evaluate the antibacterial activity of free Tet and Tet-Met-$NiFe_2O_4$ nanoparticles. Table 3 showed that MIC of Tet-Met-$NiFe_2O_4$ nanoparticles against pathogenic bacteria were between 1 to 8 μg/mL. However, Tet-Met-$NiFe_2O_4$ nanoparticles had potent antibacterial activity against Gram-negative bacteria with a significant reduction in MIC and MBC values i.e., 2–3-folds as compared to that of free Tet (Table 3). This was probably due to more penetration of Tet-Met-$NiFe_2O_4$ nanoparticles into Gram-negative bacterial cells [45]. In fact, Gram-negative bacteria possess very thin peptidoglycan layer than Gram-positive bacteria, and this structure may facilitate the penetration of nanoparticles into bacterial cells [46–49]. These data supported the idea that Met-$NiFe_2O_4$ nanoparticles can be utilized as carriers of antibiotics for antibacterial applications. Another probable antibacterial mechanism of Met-$NiFe_2O_4$ nanoparticles could be due to enhanced bacterial outer membrane permeability, which is due to the interaction of nanoparticles with the bacterial cell walls, which, in turn, alters the intrinsic membrane potential [50].

Table 3. Antibacterial activity of free Tet and Tet-Met-$NiFe_2O_4$ nanoparticles.

Bacteria		*E. coli*	*P. aeruginosa*	*S. aureus*	*E. faecalis*
MIC (μg/mL)	Free Tet	8	8	8	8
	Tet-met-$NiFe_2O_4$	1	2	4	4
MBC (μg/mL)	Free Tet	16	16	16	16
	Tet-met-$NiFe_2O_4$	2	2	8	8

4. Conclusions

MNPs have been broadly explored for the development of drug delivery systems in recent years. In this study, Tet-Met-$NiFe_2O_4$ nanoparticles was fabricated for cancer therapeutics. Results suggested that methionine coating onto magnetic $NiFe_2O_4$ nanoparticles stabilize the nanoparticles and, thus, lead to more effective drug loading. Evidently, Tet was released rapidly into the cancer cells. In vitro cytotoxicity test indicated the excellent biocompatibility of magnetic nanocarriers due to the surface coating with methionine. When Met-$NiFe_2O_4$ nanoparticles were tested, no cytotoxicity was observed on both cell lines. Tet-Met-$NiFe_2O_4$ nanoparticles showed significant cytotoxicity on A375 cells, even higher than free Tet solution.

Furthermore, strong bactericidal activity was seen, when Tet-Met-$NiFe_2O_4$ nanoparticles was tested against different Gram-positive and Gram-negative bacterial pathogens. Collectively, these results presented that Met-$NiFe_2O_4$ nanoparticles like biocompatible nanocarriers could be potentially utilized for treating bacterial infections and cancer.

Author Contributions: Conceptualization, writing—original draft preparation, writing—review and editing, supervision, and project administration, P.K.G.; writing—original draft preparation, F.E.Y.; writing—review and editing, A.E.Y., B.F.F., A.M., S.K., B.Z.S. and S.P.; supervision and project administration, V.K.T.; funding acquisition, W.F.A. All authors have read and agreed to the published version of the manuscript.

Funding: Authors wish to thank their parental institutes for providing the necessary facilities to accomplish this work. Walaa F. Alsanie would like to acknowledge Taif University TURSP program (TURSP-2020/53) for funding.

Institutional Review Board Statement: Not applicable.

Informed Consent Statement: Not applicable.

Data Availability Statement: Not applicable.

Conflicts of Interest: The authors declare no conflict of interest.

References

1. Mittal, D.; Kumar, A.; Balasubramaniam, B.; Thakur, R.; Siwal, S.S.; Saini, R.V.; Gupta, R.K.; Saini, A.K. Synthesis of Biogenic Silver Nanoparticles Using Plant Growth-Promoting Bacteria: Potential Use as Biocontrol Agent Against Phytopathogens. *Biomater. Polym. Horiz.* **2021**, *1*, 22–31. [CrossRef]
2. Sleigh, S.H.; Barton, C.L. Repurposing Strategies for Therapeutics. *Pharm. Med.* **2012**, *24*, 151–159. [CrossRef]
3. Da Cunha, E.F.F.; Ramalho, T.C.; Josa, D.; Caetano, M.S.; de Souza, T.C.S. Targeting Inhibition of COX-2: A Review of Patents, 2002–2006. *Recent. Pat. Inflamm. Allergy Drug Discov.* **2007**, *1*, 108–123. [CrossRef]
4. Behdad, R.; Pargol, M.; Mirzaie, A.; Karizi, S.Z.; Noorbazargan, H.; Akbarzadeh, I. Efflux Pump Inhibitory Activity of Biologically Synthesized Silver Nanoparticles against Multidrug-Resistant Acinetobacter Baumannii Clinical Isolates. *J. Basic Microbiol.* **2020**, *60*, 494–507. [CrossRef]
5. Hedayati Ch, M.; Abolhassani Targhi, A.; Shamsi, F.; Heidari, F.; Salehi Moghadam, Z.; Mirzaie, A.; Behdad, R.; Moghtaderi, M.; Akbarzadeh, I. Niosome-Encapsulated Tobramycin Reduced Antibiotic Resistance and Enhanced Antibacterial Activity against Multidrug-Resistant Clinical Strains of Pseudomonas Aeruginosa. *J. Biomed. Mater. Res. A* **2021**, *109*, 966–980. [CrossRef]
6. Mirzaie, A.; Peirovi, N.; Akbarzadeh, I.; Moghtaderi, M.; Heidari, F.; Yeganeh, F.E.; Noorbazargan, H.; Mirzazadeh, S.; Bakhtiari, R. Preparation and Optimization of Ciprofloxacin Encapsulated Niosomes: A New Approach for Enhanced Antibacterial Activity, Biofilm Inhibition and Reduced Antibiotic Resistance in Ciprofloxacin-Resistant Methicillin-Resistance Staphylococcus Aureus. *Bioorg. Chem.* **2020**, *103*, 104231. [CrossRef]
7. Akbarzadeh, I.; Tavakkoli Yaraki, M.; Bourbour, M.; Noorbazargan, H.; Lajevardi, A.; Sadat Shilsar, S.M.; Heidari, F.; Mousavian, S.M. Optimized Doxycycline-Loaded Niosomal Formulation for Treatment of Infection-Associated Prostate Cancer: An in-Vitro Investigation. *J. Drug Deliv. Sci. Technol.* **2020**, *57*, 101715. [CrossRef]
8. Ghafelehbashi, R.; Akbarzadeh, I.; Tavakkoli Yaraki, M.; Lajevardi, A.; Fatemizadeh, M.; Heidarpoor Saremi, L. Preparation, Physicochemical Properties, in Vitro Evaluation and Release Behavior of Cephalexin-Loaded Niosomes. *Int. J. Pharm.* **2019**, *569*, 118580. [CrossRef]
9. Ghomi, Z.; Tafvizi, F.; Naseh, V.; Akbarzadeh, I. Effect of Artemisia Ciniformis Extract on Expression of NorA Efflux Pump Gene in Ciprofloxacin Resistant Staphylococcus Aureus by Real Time PCR. *Iran. J. Med. Microbiol.* **2020**, *14*, 55–69. [CrossRef]
10. Etebu, E.; Arikekpar, I. Antibiotics: Classification and Mechanisms of Action with Emphasis on Molecular Perspectives. *IJAMBR* **2016**, *4*, 90–101.
11. Kohanski, M.A.; Dwyer, D.J.; Collins, J.J. How Antibiotics Kill Bacteria: From Targets to Networks. *Nat. Rev. Microbiol.* **2010**, *8*, 423–435. [CrossRef]
12. Padiyara, P.; Inoue, H.; Sprenger, M. Global Governance Mechanisms to Address Antimicrobial Resistance. *Infect. Dis.* **2018**, *11*, 1178633718767887. [CrossRef]
13. Singh, P.; Garg, A.; Pandit, S.; Mokkapati, V.R.S.S.; Mijakovic, I. Antimicrobial Effects of Biogenic Nanoparticles. *Nanomaterials* **2018**, *8*, 1009. [CrossRef]
14. Wu, X.; Xu, Z.; Huang, Z.; Shao, C. Large Volume Sample Stacking of Cationic Tetracycline Antibiotics toward 10 Ppb Level Analysis by Capillary Electrophoresis with UV Detection. *Electrophoresis* **2016**, *37*, 2963–2969. [CrossRef]
15. Du, F.; Zheng, X.; Sun, L.; Qin, Q.; Guo, L.; Ruan, G. Development and Validation of Polymerized High Internal Phase Emulsion Monoliths Coupled with HPLC and Fluorescence Detection for the Determination of Trace Tetracycline Antibiotics in Environmental Water Samples. *J. Sep. Sci.* **2015**, *38*, 3774–3780. [CrossRef]
16. Akbarzadeh, I.; Fatemizadeh, M.; Heidari, F.; Niri, N.M. Niosomal Formulation for Co-Administration of Hydrophobic Anticancer Drugs into MCF-7 Cancer Cells. *Arch. Adv. Biosci.* **2020**, *11*, 1–9. [CrossRef]
17. Akbarzadeh, I.; Saremi Poor, A.; Yaghmaei, S.; Norouzian, D.; Noorbazargan, H.; Saffar, S.; Ahangari Cohan, R.; Bakhshandeh, H. Niosomal Delivery of Simvastatin to MDA-MB-231 Cancer Cells. *Drug Dev. Ind. Pharm.* **2020**, *46*, 1535–1549. [CrossRef]
18. Shad, P.M.; Karizi, S.Z.; Javan, R.S.; Mirzaie, A.; Noorbazargan, H.; Akbarzadeh, I.; Rezaie, H. Folate Conjugated Hyaluronic Acid Coated Alginate Nanogels Encapsulated Oxaliplatin Enhance Antitumor and Apoptosis Efficacy on Colorectal Cancer Cells (HT29 Cell Line). *Toxicol. Vitr.* **2020**, *65*, 104756. [CrossRef]
19. Shirzad, M.; Jamehbozorgi, S.; Akbarzadeh, I.; Aghabozorg, H.R.; Amini, A. The Role of Polyethylene Glycol Size in Chemical Spectra, Cytotoxicity, and Release of PEGylated Nanoliposomal Cisplatin. *ASSAY Drug Dev. Technol.* **2019**, *17*, 231–239. [CrossRef]
20. Bhattacharyya, S.; Kudgus, R.A.; Bhattacharya, R.; Mukherjee, P. Inorganic Nanoparticles in Cancer Therapy. *Pharm. Res.* **2011**, *28*, 237. [CrossRef]
21. Ahmad, A.; Othman, I.; Md Zain, A.; Chowdhury, E. Controlled Release of Insulin in Blood from Strontium-Substituted Carbonate Apatite Complexes. *Curr. Drug Deliv.* **2015**, *12*, 210–222. [CrossRef]
22. Roca, A.G.; Carmona, D.; Miguel-Sancho, N.; Bomatí-Miguel, O.; Balas, F.; Piquer, C.; Santamaría, J. Surface Functionalization for Tailoring the Aggregation and Magnetic Behaviour of Silica-Coated Iron Oxide Nanostructures. *Nanotechnology* **2012**, *23*, 155603. [CrossRef]
23. Yiu, H.H.P. Engineering the Multifunctional Surface on Magnetic Nanoparticles for Targeted Biomedical Applications: A Chemical Approach. *Nanomedicine* **2011**, *6*, 1429–1446. [CrossRef]
24. Cheong, S.; Ferguson, P.; Feindel, K.W.; Hermans, I.F.; Callaghan, P.T.; Meyer, C.; Slocombe, A.; Su, C.-H.; Cheng, F.-Y.; Yeh, C.-S.; et al. Simple Synthesis and Functionalization of Iron Nanoparticles for Magnetic Resonance Imaging. *Angew. Chem.* **2011**, *123*, 4292–4295. [CrossRef]

25. Cho, N.H.; Cheong, T.C.; Min, J.H.; Wu, J.H.; Lee, S.J.; Kim, D.; Yang, J.S.; Kim, S.; Kim, Y.K.; Seong, S.Y. A Multifunctional Core-Shell Nanoparticle for Dendritic Cell-Based Cancer Immunotherapy. *Nat. Nanotechnol.* **2011**, *6*, 675–682. [CrossRef]
26. Farokhzad, O.C.; Langer, R. Impact of Nanotechnology on Drug Delivery. *ACS Nano* **2009**, *3*, 16–20. [CrossRef]
27. Davis, M.E.; Chen, Z.; Shin, D.M. Nanoparticle Therapeutics: An Emerging Treatment Modality for Cancer. *Nat. Rev. Drug Discov.* **2008**, *7*, 771–782. [CrossRef]
28. Sanpo, N.; Berndt, C.C.; Wang, J. Microstructural and Antibacterial Properties of Zinc-Substituted Cobalt Ferrite Nanopowders Synthesized by Sol-Gel Methods. *J. Appl. Phys.* **2012**, *112*, 084333. [CrossRef]
29. Bae, S.; Lee, S.W.; Hirukawa, A.; Takemura, Y.; Jo, Y.H.; Lee, S.G. AC Magnetic-Field-Induced Heating and Physical Properties of Ferrite Nanoparticles for a Hyperthermia Agent in Medicine. *IEEE Trans. Nanotechnol.* **2009**, *8*, 86–94. [CrossRef]
30. Naseri, M.G.; Saion, E.B.; Ahangar, H.A.; Hashim, M.; Shaari, A.H. Simple Preparation and Characterization of Nickel Ferrite Nanocrystals by a Thermal Treatment Method. *Powder Technol.* **2011**, *212*, 80–88. [CrossRef]
31. Perron, H.; Mellier, T.; Domain, C.; Roques, J.; Simoni, E.; Drot, R.; Catalette, H. Structural Investigation and Electronic Properties of the Nickel Ferrite: A Periodic Density Functional Theory Approach. *J. Phys. Condens. Matter* **2007**, *19*, 346219. [CrossRef]
32. Ling, D.; Lee, N.; Hyeon, T. Chemical Synthesis and Assembly of Uniformly Sized Iron Oxide Nanoparticles for Medical Applications. *ACC Chem. Res.* **2015**, *48*, 1276–1285. [CrossRef] [PubMed]
33. Pourgolmohammad, B.; Masoudpanah, S.M.; Aboutalebi, M.R. Synthesis of $CoFe_2O_4$ Powders with High Surface Area by Solution Combustion Method: Effect of Fuel Content and Cobalt Precursor. *Ceram. Int.* **2017**, *43*, 3797–3803. [CrossRef]
34. Wang, G.; Zhou, F.; Li, X.; Li, J.; Ma, Y.; Mu, J.; Zhang, Z.; Che, H.; Zhang, X. Controlled Synthesis of L-Cysteine Coated Cobalt Ferrite Nanoparticles for Drug Delivery. *Ceram. Int.* **2018**, *44*, 13588–13594. [CrossRef]
35. Angadi, V.J.; Choudhury, L.; Sadhana, K.; Liu, H.L.; Sandhya, R.; Matteppanavar, S.; Rudraswamy, B.; Pattar, V.; Anavekar, R.V.; Praveena, K. Structural, Electrical and Magnetic Properties of Sc^{3+} Doped Mn-Zn Ferrite Nanoparticles. *J. Magn. Magn. Mater.* **2017**, *424*, 1–11. [CrossRef]
36. Saykova, D.; Saikova, S.; Mikhlin, Y.; Panteleeva, M.; Ivantsov, R.; Belova, E. Synthesis and Characterization of Core–Shell Magnetic Nanoparticles $NiFe_2O_4$@Au. *Metals* **2020**, *10*, 1075. [CrossRef]
37. Majed, H.M.; Khalef, H.Y.; Awadh, H.A.; Noomi, B.S.; Jafar, N.A.; Hadi, K.A. Evaluation the Safety and Synergistic Effect of $NiFe_2O_4$ Nanoparticles with Antibiotic against Pseudomonas Aeruginosa. *Iraqi J. Vet. Sci.* **2021**, *35*, 71–77. [CrossRef]
38. Gheidari, D.; Mehrdad, M.; Maleki, S.; Hosseini, S. Synthesis and Potent Antimicrobial Activity of $CoFe_2O_4$ Nanoparticles under Visible Light. *Heliyon* **2020**, *6*, e05058. [CrossRef]
39. Sibuh, B.Z.; Gupta, P.K.; Taneja, P.; Khanna, S.; Sarkar, P.; Pachisia, S.; Khan, A.A.; Jha, N.K.; Dua, K.; Singh, S.K.; et al. Synthesis, In Silico Study, and Anti-Cancer Activity of Thiosemicarbazone Derivatives. *Biomedicines* **2021**, *9*, 1375. [CrossRef]
40. Kumar Trivedi, M. Spectroscopic Characterization of Chloramphenicol and Tetracycline: An Impact of Biofield Treatment. *Pharm. Anal. Acta* **2015**, *6*, 395. [CrossRef]
41. Eshrati Yeganeh, F.; Yousefi, M.; Hekmati, M.; Bikhof, M. An Experimental Research on PH-Responsive Amino Acid-Coated $Ni_{(1-x)}Co_xFe_2O_4$ Nanoparticles as a Nano-Carrier for Drug Delivery and Biological Applications. *Chem. Pap.* **2021**, *75*, 6047–6057. [CrossRef]
42. Brandenberger, C.; Mühlfeld, C.; Ali, Z.; Lenz, A.G.; Schmid, O.; Parak, W.J.; Gehr, P.; Rothen-Rutishauser, B. Quantitative Evaluation of Cellular Uptake and Trafficking of Plain and Polyethylene Glycol-Coated Gold Nanoparticles. *Small* **2010**, *6*, 1669–1678. [CrossRef] [PubMed]
43. Jamshidifar, E.; Eshrati Yeganeh, F.; Shayan, M.; Tavakkoli Yaraki, M.; Bourbour, M.; Moammeri, A.; Akbarzadeh, I.; Noorbazargan, H.; Hossein-Khannazer, N. Super Magnetic Niosomal Nanocarrier as a New Approach for Treatment of Breast Cancer: A Case Study on SK-BR-3 and MDA-MB-231 Cell Lines. *Int. J. Mol. Sci.* **2021**, *22*, 7948. [CrossRef] [PubMed]
44. Cicuéndez, M.; Doadrio, J.C.; Hernández, A.; Portolés, M.T.; Izquierdo-Barba, I.; Vallet-Regí, M. Multifunctional PH Sensitive 3D Scaffolds for Treatment and Prevention of Bone Infection. *Acta Biomater.* **2018**, *65*, 450–461. [CrossRef] [PubMed]
45. Zhang, J.; Yuan, Z.F.; Wang, Y.; Chen, W.H.; Luo, G.F.; Cheng, S.X.; Zhuo, R.X.; Zhang, X.Z. Multifunctional Envelope-Type Mesoporous Silica Nanoparticles for Tumor-Triggered Targeting Drug Delivery. *J. Am. Chem. Soc.* **2013**, *135*, 5068–5073. [CrossRef] [PubMed]
46. Abbaszadegan, A.; Ghahramani, Y.; Gholami, A.; Hemmateenejad, B.; Dorostkar, S.; Nabavizadeh, M.; Sharghi, H. The Effect of Charge at the Surface of Silver Nanoparticles on Antimicrobial Activity against Gram-Positive and Gram-Negative Bacteria: A Preliminary Study. *J. Nanomater.* **2015**, *2015*, 53. [CrossRef]
47. Yeganeh, F.E.; Yeganeh, A.E.; Yousefi, M.; Far, B.F.; Akbarzadeh, I.; Bokov, D.O.; Raahemifar, K.; Soltani, M. Formulation and Characterization of Poly (Ethylene Glycol)-Coated Core-Shell Methionine Magentic Nanoparticles as a Carrier for Naproxen Delivery: Growth Inhibition of Cancer Cells. *Cancer* **2022**, *14*, 1797. [CrossRef]
48. Sinha, S.; Sibuh, B.Z.; Mishra, A.; Pant, K.; Tomar, S.; Anand, J.; Gupta, P.K. Synthesis, Characterization and Remedial Action of Biogenic p-Ag Nanoparticles. *Nanofabrication* **2022**, 1–6. [CrossRef]
49. Thakur, N.; Anu; Kumar, K.; Thakur, V.K.; Soni, S.; Kumar, A.; Samant, S.S. Antibacterial and Photocatalytic Activity of Undoped and (Ag, Fe) co-doped CuO Nanoparticles via Microwave Assisted Method. *Nanofabrication* **2022**, 1–27. [CrossRef]
50. Losasso, C.; Belluco, S.; Cibin, V.; Zavagnin, P.; Mičetić, I.; Gallocchio, F.; Zanella, M.; Bregoli, L.; Biancotto, G.; Ricci, A. Antibacterial Activity of Silver Nanoparticles: Sensitivity of Different Salmonella Serovars. *Front. Microbiol.* **2014**, *5*, 227. [CrossRef]